

Received July 3, 2020, accepted July 26, 2020, date of publication August 4, 2020, date of current version August 14, 2020.

Digital Object Identifier 10.1109/ACCESS.2020.3014085

Negative Group Velocity Plasmons Propagating in Waveguides Composed of Graphene Metamaterials

LIQIANG ZHUO¹, SHAOJIAN SU¹, ZEYANG ZHAO¹, HENGJIE ZHOU¹, ZHEN HE¹, HUANXI MA¹, ZHILI LIN¹, (Senior Member, IEEE), AND WEIBIN QIU^{1,2}, (Senior Member, IEEE)

¹College of Information Science and Engineering, Huaqiao University, Xiamen 361021, China

²Fujian Key Laboratory of Semiconductor Materials and Applications, Xiamen 361005, China

Corresponding authors: Shaojian Su (sushaojian@hqu.edu.cn) and Weibin Qiu (wbqiu@hqu.edu.cn)

This work was supported in part by the Natural Science Fund of China under Grant 11774103, in part by the Quanzhou City Science and Technology Program under Grant 2018C003, and in part by the Open Project of the Fujian Key Laboratory of Semiconductor Materials and Applications under Grant 2019001.

ABSTRACT Fast light which demonstrates negative group velocity, is achieved by the anomalous dispersion or photon tunneling. However, many applications based on the fast light are limited due to the disadvantages of inferior tunability or nonlinear dispersion relationship of the fast light-carrying medium. In this paper, we propose the graphene plasmonic crystal waveguides whose guiding and claddings are composed of the graphene plasmonic metamaterials, where the backward propagating plasmonic modes corresponding to negative group velocity are observed. The dispersion relation and the group velocity of three types of graphene plasmonic crystal waveguides are investigated by varying the materials and the geometrical parameters of the graphene plasmonic crystal waveguides. Numerical experiments are designed to verify the authenticity of a fast plasmon in the graphene plasmonic crystal waveguides. Our proposed graphene plasmonic crystal waveguides might find significant applications in the fields of nanophotonics, on-chip electromagnetic field manipulation in deep nanoscale, and the technique of high density plasmonic integrated plasmonic circuit in the future.


INDEX TERMS Plasmonic waveguides, metamaterials, negative group velocity, anomalous dispersion, graphene plasmonic crystals.

I. INTRODUCTION

Fast light refers to the electromagnetic wave which travels faster than the speed of light c in a vacuum or takes a negative value of the group velocity v_g [1]. This circumstance can occur for $v_g = c/n_g$ being superluminal as well as infinite or negative, where n_g is the group refractive index [2], [3]. Superluminal group velocity has been realized by photon tunneling based on the evanescent state [4], [5][Boyd, 2001 #2; Bolda, 1993 #4; Heitmann, 1997 #7], barrier traversal [6], and superluminality of Bessel-X waves [7]–[9], etc. In recent years, G. Gehring et al reported the negative group velocity of light by using the anomalous dispersion caused by asymmetric gain and absorption lines [10]–[13], [10], [11]. Furthermore, because v_g has extraordinary significance and value (v_g is the speed at which the signal (or information) is

transmitted as long as it is invariant (impulse is not distorted) in the specified frequency band) [14], [15], fast light has excellent prospects and potential applications in optical communication systems, such as data pulse buffering, regeneration [16], [17], detection of gravitational waves [17]–[19] and implementation of robust storage [20], [21]. It's worth noting that, nevertheless, the reported structures are limited by the mediocre tunability and the nonlinear dispersion relationship, which hinders its development in integrated and micro-nano optical systems. Therefore, the structures with excellent tunability and linear dispersion relation are highly desired.

Graphene, a hexagonal honeycomb lattice flat film composed of nanolayer carbon atoms with sp^2 -hybridized orbitals, is a two-dimensional nanomaterial with a carbon atom thickness [22], [23]. Since the graphene monolayer was fabricated, it has been widely studied for its promising applications in various fields [24]. Graphene is the basic building block of graphite materials in all other dimensions, which

The associate editor coordinating the review of this manuscript and approving it for publication was Leo Spiekman .

can be packaged as zero-dimensional (0D) fullerenes, rolled into one-dimensional (1D) nanotubes or stacked into three-dimensional (3D) graphite [22], [25]. Graphene-supported surface plasmon polaritons (SPPs), besides, offer advantages such as tight field confinement, relatively low propagation loss, and flexible tunability [26]–[30]. Furthermore, on account of its metal-like properties at terahertz (THz) and infrared wavelengths, the graphene is widely considered as an ideal material for plasmonic devices [31], [32]. Graphene plasmonic crystals (GPCs), in special, are a kind of graphene-based metamaterial with excellent tunability and linear dispersion relationship. Negative permittivity and permeability can be obtained based on the linear dispersion relationship around the Dirac-like point (DLP). In this case, GPCs act as negative-index materials (NIMs), also known as left-handed materials (LHMs). Although conventional dielectric photonic crystals (PhCs) also offer this property, the frequency of the DLP cannot be modulated once the lattice structure of the PhCs and the parameters of the dielectric materials are determined. Thus, conventional dielectric PhC systems typically possess very limited tunability [33]. On the contrary, due to the excellent tunability of graphene chemical potential, GPCs can realize the adjustment of DLP's frequency. Recently, L. Xiong et al have implemented GPCs experimentally and demonstrated the potential applications in the fields of integrated, micro-nano optics and on-chip light manipulation [34].

In this paper, we first investigate the normalized dispersion relation of three types of waveguide with anomalous dispersion curves. Then, a graphene plasmonic crystal structure is designed and the band structure and electromagnetic field distribution are studied. The effective permittivity and permeability of the plasmonic crystal near DLP climb from negative to positive continuously and linearly. This graphene-based plasmonic crystal is used as the LHMs or right-handed materials (RLMs) with different structure parameters or operating frequency. Most importantly of all, we propose a graphene plasmonic crystal waveguide (GPCW), which consists of a guiding layer sandwiched by cladding layers, all three layers are made up of GPCs. The negative (or positive) equivalent refraction index is obtained by properly designing the structure of the GPCs. Thus, three types of GPCW are constructed by using the graphene metamaterials. Then, we explore the fast light phenomenon in the proposed nanostructures. Finally, numerical propagation experiments are utilized to verify the negative group velocity (fast light) caused by the anomalous dispersion.

II. THREE SYMMETRIC WAVEGUIDES CONTAINING NIMs

For simplicity, hereafter, the material with both positive relative permittivity and relative permeability is referred to as RHM, while the material with both negative relative permittivity and relative permeability is referred to as LHM. GPCW composed of RHM guiding layer and LHM claddings is named LRL. Similarly, RLR and LLL types of waveguides are defined in the same way. The symmetric waveguide

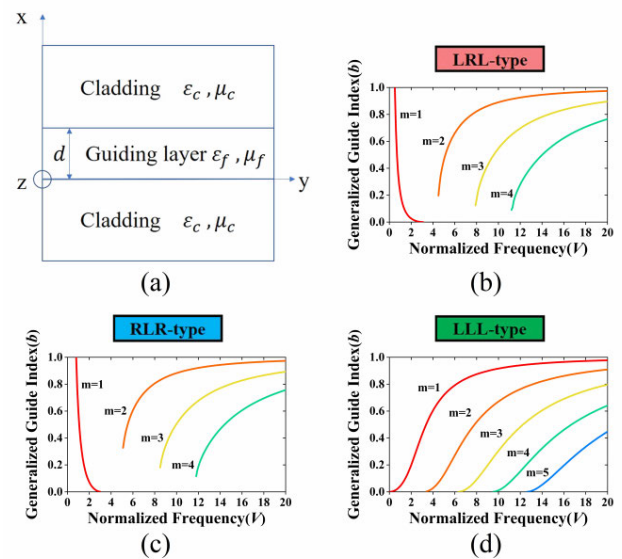


FIGURE 1. Schematic of the symmetric waveguide and the normalized dispersion curves. (a) The geometry of a three-layer symmetric waveguide. (b) Normalized dispersion curves for TM modes (applied to all the following) for a LRL symmetric waveguide with RHM core and LHM claddings. $\mu_f/\mu_c = -4$. (c) Normalized dispersion curves for a RLR symmetric waveguide with RHM claddings and LHM core. $\mu_f/\mu_c = -2.5$. (d) Normalized dispersion curves for a LLL symmetric waveguide with both LHM core and claddings. $\mu_f/\mu_c = 4$.

structure, as shown in Fig. 1(a). We construct three types of symmetric waveguide structures using NIMs: LRL, RLR, and LLL. Take the LRL waveguide for example, it is composed of a dielectric RHM core containing the relative permittivity ϵ_f and the relative permeability μ_f and taking up the region $0 < x < d$ sandwiched between two dielectric LHM claddings (ϵ_c, μ_c) occupying the region $-\infty < x < 0$ and $d < x < +\infty$, respectively. The claddings are assumed to be uniform dielectric LHMs with identical ϵ_c and μ_c . The refractive index of the core and cladding are expressed as severally $n_f = (\epsilon_f \mu_f)^{1/2}$ and $n_c = (\epsilon_c \mu_c)^{1/2}$. Similarly, the RLR and LLL waveguide have a parallel composition to the LRL waveguide, except for differences in the choice of materials for the core and cladding.

First of all, to obtain the dispersion characteristic curve for TM modes of the LRL, RLR, and LLL waveguides conveniently, we introduce two parameters to describe the guided modes. The first one is the normalized frequency V given by

$$V = k_0 d \sqrt{n_f^2 - n_c^2}, \quad (|n_f| > |n_c|), \quad (1)$$

and the second one is the generalized guide index b given by

$$b = \frac{N^2 - n_c^2}{n_f^2 - n_c^2}, \quad (2)$$

where k_0 is the wavenumber in free space, N represents the effective mode refraction of the waveguide. Utilizing these parameters and applying the continuous boundary conditions, we obtain the following dispersion relation equation for TM

modes

$$V\sqrt{1-b} = 2\tan^{-1}\frac{\mu_f}{\mu_c}\sqrt{\frac{b}{1-b}} + m\pi, \quad (3)$$

where m is the mode order. This dispersion relation describes the relationship between V and b , and we cope with the case of LRL waveguide with $\mu_f/\mu_c = -4$, Fig.1(b) plots b as a function of V , where the first four orders of modes are included, which are known as the normalized dispersion. When the mode order $m = 1$, the dispersion relation between V and b ($\partial b/\partial V < 0$) is defined as anomalous dispersion as well as quite different from it for $m > 1$. Moreover, the dispersion relation in the RLR waveguides also has similar anomalous dispersion, as shown in Fig. 1(c). The fast light phenomenon can be induced due to the anomalous dispersion, and the group velocity of optical pulses is greater than the speed of light in a vacuum or is negative. We use graphene metamaterials, whose effective refractive index could be positive or negative with respect to the frequency, to construct LRL and RLR symmetric slab waveguide, and numerically verify the fast light characteristics.

However, as depicted in Fig. 1(d), there is no anomalous dispersion in the dispersion relation of LLL waveguide with $\mu_f/\mu_c = 4$ solve by (3). Its first five orders of modes are all normal dispersion, containing a fundamental mode ($m = 0$) without cutoff frequency. We also construct LLL waveguide with anomalous dispersion and no cutoff frequency by using the graphene metamaterials.

III. GRAPHENE PLASMONIC CRYSTALS WITH SQUARE UNIT CELL STRUCTURE

A. THE EFFECTIVE REFRACTIVE INDEX OF PLASMON SUPPORTED BY GRAPHENE MONOLAYER

As shown in Fig. 2(a), the 2D GPCs presented in our work consist of graphene nanodisk array arranged in a square lattice, which can be achieved by periodically adjusting the chemical potential of a single layer of graphene. Specifically, the chemical potential of graphene can be effectively tuned via chemical doping or external gate voltage [28], [31]. The profile of 2D GPCs is illustrated in Fig. 2(b). When the external gate bias voltage is applied between the graphene sheet and the silicon substrate, periodical distribution of the chemical potential of the graphene sheet is obtained due to the periodical distribution of the thickness of the silica layer. The chemical potential ratio μ_{c1}/μ_{c2} between two graphene regions with silica thicknesses d_1 and d_2 (Fig. 2(b)) under an external gate voltage is equal to $(d_1/d_2)^{1/2}$ [35].

We solve the Maxwell equations according to the boundary conditions, and then deduce the dispersion of the SPP modes, which is given by the following equation [36]:

$$\frac{\varepsilon_{Air}}{\sqrt{\beta^2 - k_0^2\varepsilon_{Air}}} + \frac{\varepsilon_{Silica}}{\sqrt{\beta^2 - k_0^2\varepsilon_{Silica}}} = \frac{\sigma_g}{i\omega\varepsilon_0}, \quad (4)$$

where $\varepsilon_{Air} = 1$ and $\varepsilon_{Silica} = 3.9$ respectively represent the relative permittivity of air and silica corresponding to super and substrates. i , ω , and ε_0 stand for the imaginary

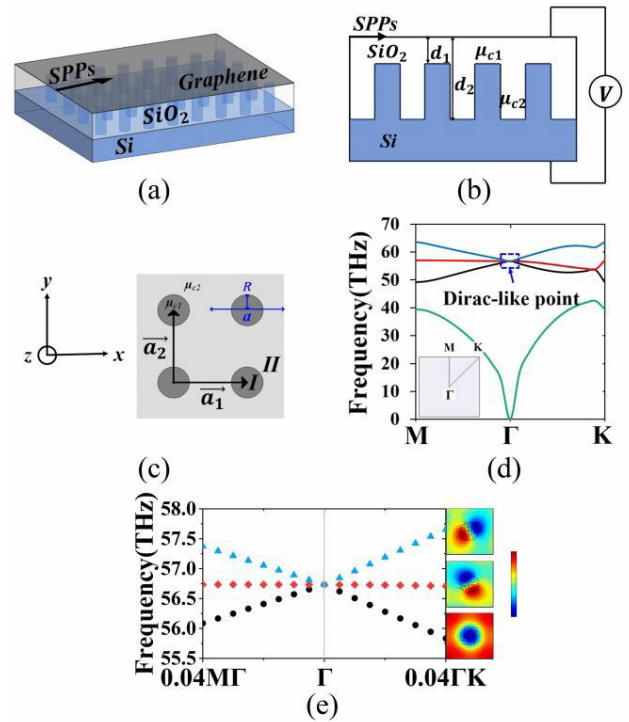


FIGURE 2. Schematic diagram of the Graphene plasmonic crystals (GPCs) and the band structure. (a) 3D-schematic diagram of the GPCs.

(b) 2D-profile diagram of the GPCs. The chemical potential of graphene is periodically modified by using a silica layer with a periodic thickness. With an external gate voltage, the graphene regions of the silica layers with periodic thicknesses d_1 and d_2 corresponding to periodic chemical potentials μ_{c1} and μ_{c2} , and the chemical potential ratio is $\mu_{c1}/\mu_{c2} = (d_1/d_2)^{1/2}$. (c) Schematic configuration of the surface of square lattice GPCs in real space. The chemical potential of the graphene nanodisk (region I) and the background graphene (region II) are μ_{c1} and μ_{c2} respectively. We set $a_1 = a_2 = a$ as the lattice constant and R as the radius of the graphene nanodisk. (d) The band structure of the GPC with $a = 60$ nm, $R = 0.21527a$, $\mu_{c1} = 0.3$ eV, $\mu_{c2} = 0.8$ eV. Inset: first Brillouin zone (FBZ). (e) Detail information of the triplet degenerate Bloch states around the DLP and the corresponding electromagnetic field modes. Dark red and dark blue represent the positive and negative maximum values of the field E_z , respectively. The black arrow represents the magnetic field vector in the plane whose magnitude is proportional to the length of the arrow. The blue and the red dot line correspond to the dipole mode and black dot line to the monopole mode.

unit, the angular frequency of the plasmon, and the vacuum permittivity of free space, respectively. $k_0 = 2\pi/\lambda$ is the vacuum wave number in free space. When $k_0 \ll \beta$, (4) is simplified to

$$\beta = \varepsilon_0 \frac{\varepsilon_{Air} + \varepsilon_{Silica}}{2} \frac{2i\omega}{\sigma_g}. \quad (5)$$

Here, according to the Kubo formula [37], [38], the surface conductivity of graphene σ_g is composed of the contributions from inter-band electron transitions σ_{inter} and the intra-band electron-phonon scattering σ_{intra} ,

$$\begin{aligned} \sigma_g &= \sigma_{intra} + \sigma_{inter}, \\ \sigma_{intra} &= \frac{ie^2k_B T}{\pi\hbar^2(\omega + i/\tau)} \left[\frac{\mu_c}{k_B T} + 2\ln\left(1 + \exp\left(-\frac{\mu_c}{k_B T}\right)\right) \right], \end{aligned} \quad (6)$$

$$\sigma_{inter} = \frac{ie^2}{4\pi\hbar} \ln \left(\frac{2|\mu_c| - (\omega + i/\tau)}{2|\mu_c| + (\omega + i/\tau)} \right). \quad (8)$$

The constants e , k_B , and \hbar denote the electron charge, the Boltzmann constant, and the reduced Planck constant, respectively. σ_{inter} and σ_{intra} are controlled by the operating temperature T , chemical potential μ_c , the angular frequency of the plasmon ω , and electron momentum relaxation time τ . The effective complex refractive index of SPP modes on the graphene layer is expressed as $n_{eff} = \beta/k_0$. It is worth noting that the surface conductivity of graphene, which determines the propagation constant of SPP modes on the graphene layer, depends mainly on the chemical potential. The complex effective refractive index of SPP modes on the graphene layer is rewritten by $n_{eff} = n + ik$, where the imaginary part of the complex index k is the effects of absorption and radiation losses.

B. THE BAND STRUCTURE OF GPCs

Fig. 2(c) illustrates the unit cell of the GPCs, where the graphene nanodisk with a radius R has a chemical potential μ_{c1} which is surrounded by the ambient chemical potential μ_{c2} . The plasmonic crystal is arranged in a square lattice with lattice constants a . The photonic band structure of the GPCs is obtained by numerically solving the Maxwell equations. When the graphene nanodisks with $\mu_{c1} = 0.3$ eV are immersed in the ambient graphene with $\mu_{c2} = 0.8$ eV, $a = 60$ nm and $R = 0.21527a$. The band structure is numerically calculated by COMSOL Multiphysics based on the finite-element method (FEM), and the band structure of that GPC along with the M - Γ - K path of the reduced BZ is depicted in Fig. 2(d). In this band structure, there are two independent Bloch eigenstates at point Γ to represent the relationship between frequency and wave vector k , i.e., a singleton and a dual degenerate state corresponding to a single monopole and two dipole modes, respectively.

Fig. 2(e) shows the detailed information of the band structure near point Γ , in which two bands intersect linearly at the degenerate point of Γ , and a flat band passes through this point. When the radius R of graphene nanodisk is adjusted to $0.21527a$, the singlet and the dual degeneracy merge at point Γ , with occasional degeneracy occurring, then this triply degenerate state is a Dirac-like cone at the frequency of 56.733 THz. The right side of Fig. 2(e) are the electromagnetic field modes of the three bands. The blue and the red dot line correspond to the dipole mode and black dot line to the monopole mode.

C. EFFECTIVE PERMITTIVITY AND PERMEABILITY OF THE GPCs

The effective permittivity ε_{GPCs} and the effective permeability μ_{GPCs} of GPCs vary with photon frequency and linearly vary over a small frequency range near DLP. Therefore, ε_{GPCs} and μ_{GPCs} in the selected frequency range can be regarded as a linear function of frequency. The expressions of these two

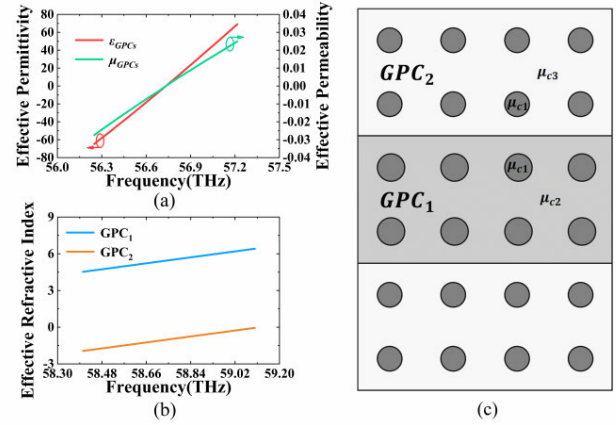


FIGURE 3. (a) The effective permittivity and permeability of the GPC₁ ($\mu_{c1} = 0.3$ eV, $\mu_{c2} = 0.8$ eV). (b) The refractive indices of the GPC₁ ($\mu_{c1} = 0.3$ eV, $\mu_{c2} = 0.8$ eV) and the GPC₂ ($\mu_{c1} = 0.3$ eV, $\mu_{c2} = 0.93$ eV). (c) Schematic configuration of the LRL-type GPCW composed of GPC₁ and GPC₂.

effective parameters are respectively given by [39]

$$\varepsilon_{GPCs}(\omega) = \frac{k}{\omega} \frac{1}{\varepsilon_0} \frac{\bar{E}_z}{\bar{H}_x} \quad (9)$$

$$\mu_{GPCs}(\omega) = \frac{k}{\omega} \frac{1}{\mu_0} \frac{\bar{H}_x}{\bar{E}_z} \quad (10)$$

where k is the wave vector, ω is the angular frequency, ε_0 and μ_0 represent the permittivity and permeability of the free space, \bar{E}_z is the average value of the eigen electric field along the z-axis and \bar{H}_x is the average value of the eigen magnetic field along the x-axis.

Based on the numerical calculation of the above two formulas, we plot The effective permittivity ε_{GPCs} and the effective permeability μ_{GPCs} as a function of frequency for the unit cell of GPCs ($\mu_{c1} = 0.3$ eV, $\mu_{c2} = 0.8$ eV), which are shown in Fig. 3(a). When the frequency is smaller (or bigger) than 56.733 THz, the effective permittivity and effective permeability are both negative (or positive) value. Thus, the refractive index of the GPCs $n_{GPCs}(\omega) = (\varepsilon_{GPCs}(\omega)\mu_{GPCs}(\omega))^{1/2} < (>) 0$, and the GPCs exhibit the properties of LHM (or RHM). Moreover, as it is mentioned above, the frequency of the Dirac-like point is tunable by modulating the chemical potential.

The LRL-type GPCW is illustrated in Fig. 3(c). Keeping μ_{c1} constant and modulating μ_{c2} to 0.93 eV, the GPCs' frequency of the Dirac-like point switch to 59.12 THz. Fig. 3(b) shows the refractive indices of GPC₁ ($\mu_{c1} = 0.3$ eV, $\mu_{c2} = 0.8$ eV) and GPC₂ ($\mu_{c1} = 0.3$ eV, $\mu_{c2} = 0.93$ eV) in the frequency range between 58.39 and 59.11 THz. In this range, the GPC₂ has a negative refractive index and is used as a LHM, whereas the GPC₁ is a RHM. Therefore, the GPC₁ can be constructed as the claddings of the LRL-type GPCW, and the guiding layer can be composed of the GPC₂. The RLR-type waveguide can be similarly constructed from a GPC₃ ($\mu_{c1} = 0.3$ eV, $\mu_{c2} = 0.79$ eV) claddings and a guiding layer made up of GPC₄ ($\mu_{c1} = 0.3$ eV, $\mu_{c2} = 0.82$ eV)

in the frequency range between 56.54 THz and 56.74 THz. Attributing to the characteristics of the effective permittivity and effective permeability varying with the frequency of the plasmons and the excellent tunability of chemical potential, the LRL, RLR, and LLL-type GPCs waveguides (GPCW) can be constructed by using the GPCs.

IV. NUMERICAL ANALYSIS OF THE DISPERSION RELATION AND DEMONSTRATION OF THE FAST LIGHT PROPAGATING IN THE GPCW

A. THE DISPERSION RELATION OF THE GPCW

As mentioned in Section II, considering the symmetric waveguide, we solve the normalized dispersion equation by introducing the normalized parameters V and b , then obtain the dispersion relation (3). However, since the GPCs that made up the whole GPCW are dispersive materials, the dispersion formula (3) in the GPCW is modified accordingly. In the GPCW, the generalized parameters are rearranged into normalized frequency V and generalized guide index b which are respectively given by

$$V = k_0(\omega) d \sqrt{n_{GPC1}^2(\omega) - n_{GPC2}^2(\omega)} \quad (|n_{GPC1}| > |n_{GPC2}|) \tag{11}$$

$$b = \frac{N_{eff}^2 - n_{GPC2}^2(\omega)}{n_{GPC1}^2(\omega) - n_{GPC2}^2(\omega)} \tag{12}$$

where the $N_{eff} = \beta/k_0(\omega)$ indicates the effective mode refraction of the GPCW. The equation the dispersion relation for SPP modes has become the following form:

$$V \sqrt{1 - b} = 2 \tan^{-1} \left[\frac{\mu_{GPC1}(\omega)}{\mu_{GPC2}(\omega)} \sqrt{\frac{b}{1 - b}} \right] + m\pi \tag{13}$$

where the normalized frequency V is regarded as a function of SPPs' frequency ω and width of guiding layer d . Based on the dispersion equation, we study how the effective mode refraction and the group velocity v_g of SPPs in the LRL-, RLR- and LLL-type GPCW vary with the frequency at different d .

B. THE EFFECTIVE MODE REFRACTION AND THE GROUP VELOCITY OF THE PLASMONS IN THE PROPOSED GPCW

Considering the LRL-type GPCW and the RLR-type GPCW with SPPs traveling through the guiding layer at d is 240 nm, 300 nm, 360 nm, and 420 nm, respectively, we plot the variation of the effective mode refraction and group velocity of plasmons as a function of frequency. In Fig. 4(a), the dispersion relation corresponds with N_{eff} versus ω for four different widths of guiding layer d composed of GPCs ($\mu_{c1} = 0.3$ eV, $\mu_{c2} = 0.8$ eV) in LRL-type GPCW ($m = 1$) is exhibited. For this type of GPCW with a certain guiding width d , N_{eff} decreases with the increasing of ω . So it is regarded as the anomalous dispersion. Moreover, when d is from 240 nm to 420 nm, for a given frequency, N_{eff} decreases with the increasing guiding layer width d . In the RLR-type GPCW, for a given frequency, the effective mode refraction

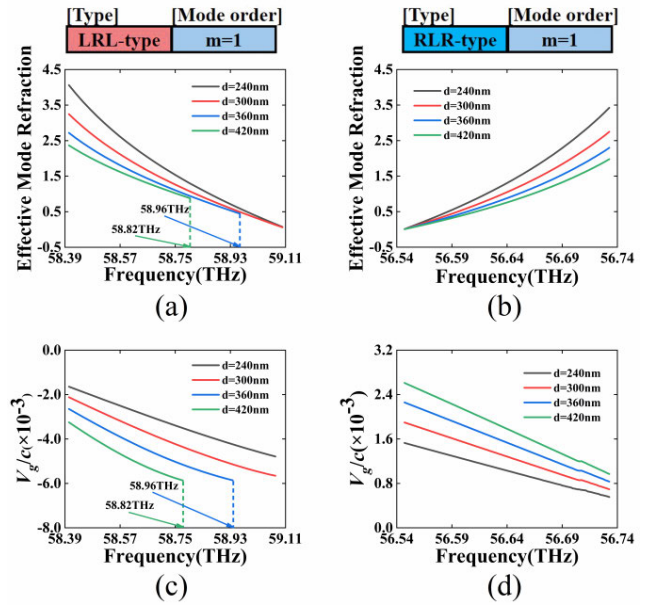


FIGURE 4. (a) The effective mode refraction of the SPPs mode in the proposed LRL-type GPCW with the adjustment of d from 240 nm to 420 nm at mode order $m = 1$. (b) The effective mode refraction of the SPPs mode in the proposed RLR-type GPCW with the variation of d from 240 nm to 420 nm at mode order $m = 1$. (c) The group velocity of SPPs mode in the proposed LRL-type GPCW with the different d . (d) The group velocity of SPPs mode in the proposed RLR-type GPCW with the different d .

index decreases with the increasing guiding layer width d . However, N_{eff} increases with the photon frequency ω , and therefore it corresponds to the normal dispersion, as shown in Fig. 4(b).

The relation between the group velocity v_g , which is defined by $v_g = d\omega/d\beta$, where β is the propagation constant, and the photon frequency ω is further investigated. For the fast light phenomenon caused by the anomalous dispersion in the LRL-type GPCW, the group velocity as a function of the photon frequency ω is illustrated in Fig. 4(c). As ω increases, the group velocity decreases in a frequency range from 58.39 THz to 59.11 THz. The group velocity v_g is always negative, indicating the existence of the backward SPP modes caused by the anomalous dispersion. Nevertheless, in the RLR-type waveguide, the group velocity is always positive and decreases with the frequency shown in Fig. 4(d). Based on the numerical results in Fig. 4, we simulate and calculate the working conditions of LRL- and RLR- type GPCW. The dynamic state of light fields of backward propagation (LRL) and forward propagation (RLR) are exhibited in the online Supplementary Materials. In addition, d has the opposite effect on the group velocity in the two waveguides, so d can be adjusted to control the group velocity in a certain frequency range. It is a remarkable fact that, when d is 360 nm, the effective mode refraction N_{eff} has no solution in the frequency range of 58.96 THz - 59.11 THz for the LRL-type GPCW, meaning that there is a forbidden band in this range. When d is 420 nm, the cut-off frequency ranges from 58.82 THz to 59.11 THz. With the constant operating

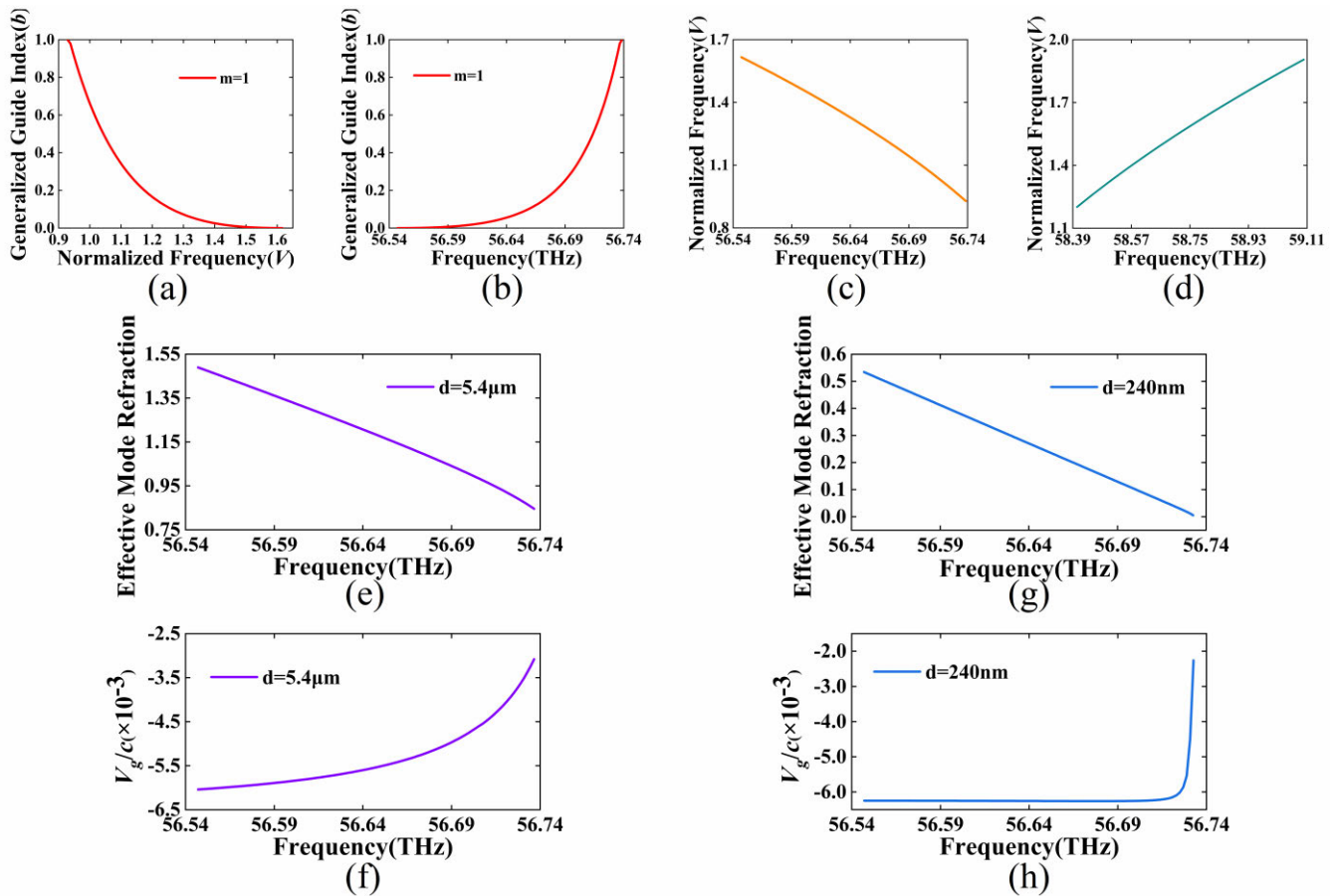


FIGURE 5. (a) Normalized dispersion curve for SPPs mode for the proposed RLR-type GPCW at $m = 1$. (b) Graph of Generalized guide index b as a function of the photon frequency ω . (c) Normalized frequency V vs. the photon frequency ω for the proposed RLR-type GPCW. (d) Normalized frequency V vs. the photon frequency ω for the proposed LRL-type GPCW. (e) The effective mode refraction in the proposed RLR-type GPCW with $d = 5.4 \mu\text{m}$ at $m = 2$. (f) The group velocity of plasmon mode in the proposed RLR-type GPCW with $d = 5.4 \mu\text{m}$. (g) The effective mode refraction in the proposed LLL-type GPCW with $d = 240 \text{ nm}$ at $m = 0$. (h) The group velocity of plasmon mode in the proposed LLL-type GPCW with $d = 240 \text{ nm}$ at $m = 0$.

frequency range of the GPCW, the wider d is, the larger the range of cut-off frequency is. Therefore, to avoid the cut-off frequency, the width of the guiding layer d should be reasonable when modulating the waveguide structure.

It is noted that the anomalous dispersion exists in LRL symmetric waveguide but vanishes in RLR-type GPCW. As shown in Fig. 5(a) and (b), though the normalized anomalous dispersion for RLR-type GPCW at $m = 1$ still exists, the trend of the generalized guide index b over the normalized frequency V is contrary to the trend of the generalized guide index b over the frequency ω . The reason is that there is a competitive relationship between the wavenumber $k_0(\omega)$ and $(n_{GPC1}^2(\omega) - n_{GPC2}^2(\omega))^{1/2}$ (marked $\delta n(\omega)$) in (11). Not only $k_0(\omega)$ and $\delta n(\omega)$ both change with the variation of the photon frequency ω , but also ω increases when d is unchanged, then $k_0(\omega)$ increases and $\delta n(\omega)$ decreases. It means that the relationship between the normalized frequency V and the photon frequency ω depends on which $k_0(\omega)$ or $\delta n(\omega)$ dominates. Therefore, for the RLR-type GPCW, $\delta n(\omega)$ dominates in the competition with $k_0(\omega)$, resulting in the reverse change of the normalized frequency V and the photon frequency ω illustrated in Fig. 5(c), while the anomalous dispersion

of $m = 1$ becomes the normal dispersion instead. On the contrary, as shown in Fig. 5(d), the normalized frequency V is proportional to the photon frequency ω in the LRL-type GPCW, which is why the anomalous dispersion still exists in the LRL-type GPCW.

C. SWITCHING THE GROUP VELOCITY BETWEEN POSITIVE AND NEGATIVE AT THE SAME FREQUENCY ON THE GPCW BY MODIFYING THE CHEMICAL POTENTIALS

According to the above analysis, when $\delta n(\omega)$ decreases with increasing the photon frequency ω and dominates the competition with $k_0(\omega)$, adjusting d can switch the normal dispersion relation at $m \geq 2$ for RLR-type GPCW to anomalous dispersion. Therefore, based on the original RLR-type GPCW, we adjusted $d = 5.4 \mu\text{m}$ at $m = 2$. The effective mode refraction N_{eff} and the group velocity v_g as a function of frequency ω are shown in Fig. 5(e) and (f). As shown in Fig. 5(e), N_{eff} is a subtractive function of ω that satisfies the anomalous dispersion, and the group velocity v_g presented in Fig. 5(f) is always negative. Although in the RLR-type GPCW we can get the backward SPPs mode corresponding to anomalous dispersion, d needs to be adjusted to $5.4 \mu\text{m}$.

Next, we build the LLL-type GPCW. If the LLL-type GPCW is constructed by using GPCs with appropriate parameters, $\delta n(\omega)$ may dominate the competition with $k_0(\omega)$, leading to that backward fundamental SPPs mode exist corresponding to anomalous dispersion. It is noticeable in Fig. 1(d), at $m = 0$, there is no cut-off frequency similar to that in LRL-type GPCW. Thus, the claddings of LLL-type GPCW are composed of GPC₁ ($\mu_{c1} = 0.3$ eV, $\mu_{c2} = 0.8$ eV), while the guiding layer is composed of GPC₄ ($\mu_{c1} = 0.3$ eV, $\mu_{c2} = 0.82$ eV), and its operating frequency is selected to the left of the Dirac-like points of the two GPCs, from 56.54 THz to 56.74 THz. The variation trends of the effective mode refraction N_{eff} (Fig. 5(g)) and group velocity v_g (Fig. 5(h)) in the frequency range from 56.54 THz to 56.74 THz are similar to those in Fig. 5(e) and (f), with the difference that d is more flexible, the waveguide parameter structure is more reasonable. The dynamic state of light fields of backward propagation (LLL) is also exhibited in the online Supplementary Materials. In addition, thanks to the excellent tunability of the GPCs and the reasonable design of the waveguide structure, the proposed LLL-type and RLR-type GPCW can switch to each other by changing only the chemical potential of the GPCs without changing geometrical structure, enabling them to have the same operating frequency range. Therefore, this can switch the fast and the normal plasmons at the same frequency, as well as make it possible to integrates an on-chip fast light device.

D. NUMERICALLY EXPERIMENTAL VERIFICATION OF THE NEGATIVE GROUP VELOCITY IN THE GPCW

For the group velocity, what we are interested in is the backward transmission (fast light phenomenon) caused by the anomalous dispersion, which is the scenario of the negative group velocity. Therefore, in this section, the methods commonly used in modern optical subsystems to judge fast light in fiber are introduced to verify the fast light phenomenon in the proposed GPCW. In order to do this, another definition of the group velocity needs to be introduced, which can be simply written as $v_g = c/n_g$, where n_g is the group refraction index. For the GPCW of length L , a Gaussian pulse of a given frequency traversing it requires $T_G = L/v_g = n_g \cdot L/c$ propagation time. There is a time difference $\Delta T = L/(v_g - L/c) = (n_g - 1) \cdot L/c$ between the elapsed time of the Gaussian pulse passing through the GPCW and the time $T_V = L/c$ that the Gaussian pulse passes the vacuum of the same length L . When ΔT is negative, it means that the group velocity is negative or greater than the velocity of vacuum light, i.e. fast light phenomenon exists. The specific experimental process is clearly illustrated in Fig. 6(a). First, the modulated Gaussian pulse is incident from the guiding layer of the GPCW with a length of L , and the output Gaussian pulse is received on the other side. Second, measure the Gaussian pulse traversing the GPCW time T_G and calculate the time $T_V = L/c$ and $\Delta T = T_G - T_V$. Next, the numerical experimental data is taken into $n_g = \Delta T \cdot c/L + 1$ to fit the experimental n_g , and the group velocity calculated by

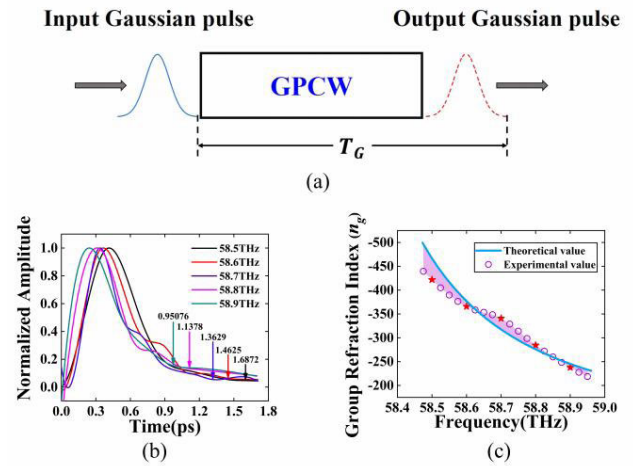


FIGURE 6. Numerically experimental results for verifying the negative group velocity in the proposed GPCW. (a) Schematic diagram of fast light verification numerical experiment. (b) Recorded output Gaussian signal waveforms have been normalized with five different frequency of input signals. (c) Comparison of theoretical and numerically experimental values of group refraction index n_g . The mauve area is the error range between the theoretical value and the experimental value.

the previous numerical simulation is used to calculate the theoretical n_g through $n_g = c/v_g$. Finally, we compare the difference between experimental n_g and theoretical n_g and conduct error analysis. Specifically, we select the proposed LRL-type GPCW with $d = 240$ nm and $L = 1.2 \mu\text{m}$ for the experiment because the group velocity in LRL-type GPCW is negative and varies significantly with the frequency. From 58.475 THz to 58.950 THz, twenty frequency points are selected as the frequency of Gaussian pulses at equal intervals. The modulated Gaussian pulses of twenty different frequencies are tested separately. Fig. 6(b) shows the normalized amplitudes of five representative outputting Gaussian pulses with different frequencies (are 58.5 THz, 58.6 THz, 58.7 THz, 58.8 THz, and 58.9 THz, respectively) recorded on the other side of the LRL-type GPCW. According to Fig. 6(b), the higher the frequency of the Gaussian pulse, the earlier time to the peak of the Gaussian pulse of the experiment. The time of the Gaussian pulses passing through the LRL-type GPCW is also marked with different colored arrows. A comparison of the experimental n_g and the theoretical n_g is demonstrated in Fig. 6(c). Both theoretical n_g and experimental n_g increase with the increase of incident Gaussian pulse frequency. This indicates that the theoretical n_g and the experimental n_g have the same variation trend in this frequency range. Though the numerically experimental n_g agrees well with theoretical n_g in general, there is still some error in certain frequencies. The mauve area in Fig. 6(c) is the error range between the theoretical value and the experimental value. These experimental errors may be due to GPCs' own scattering and weak absorption. This can affect the experimental value slightly but not the overall trend of the experimental value changing with frequency. Therefore, this numerical experiment verifies that fast plasmon exists in the proposed GPCW.

V. CONCLUSION

In summary, we proposed plasmonic waveguides constructed by graphene metamaterials, and obtained the LRL- and RLR-type GPCWs, which offer the anomalous dispersion. Backward propagating SPPs (fast plasmons) corresponding to a negative group velocity has been demonstrated, with appropriate guiding layer thickness d and mode order. In addition, for LRL-type GPCW, the cut-off frequency appears when d is too wide. In order to avoid the cut-off frequency, on the one hand, reasonable design d can be adopted. On the other hand, LLL-type GPCW with backward fundamental SPPs mode without cut-off frequency is designed by using the competition relationship between parameters. Finally, numerical experiments have been designed to verify the fast light phenomenon in the proposed GPCW.

REFERENCES

- [1] P. W. Milonni, *Fast Light, Slow Light and Left-Handed Light*. Boca Raton, FL, USA: CRC Press, 2004.
- [2] R. W. Boyd and D. J. Gauthier, "Slow and fast light," *Prog. Opt.*, vol. 43, pp. 363–385, 2001.
- [3] E. L. Bolda, R. Y. Chiao, and J. C. Garrison, "Two theorems for the group velocity in dispersive media," *Phys. Rev. A, Gen. Phys.*, vol. 48, no. 5, 1993, Art. no. 3890.
- [4] G. Nimtz and W. Heitmann, "Superluminal photonic tunneling and quantum electronics," *Prog. Quantum Electron.*, vol. 21, no. 2, pp. 81–108, Jan. 1997.
- [5] K. Wynne and D. A. Jaroszynski, "Superluminal terahertz pulses," *Opt. Lett.*, vol. 24, no. 1, pp. 25–27, 1999.
- [6] A. Enders and G. Nimtz, "On superluminal barrier traversal," *J. Phys.*, vol. 2, no. 9, pp. 1693–1698, Sep. 1992.
- [7] J. Durmin, J. J. Miceli, and J. H. Eberly, "Diffraction-free beams," *Phys. Rev. Lett.*, vol. 58, no. 15, p. 1499, 1987.
- [8] J. Durmin, "Exact solutions for nondiffracting beams. I. The scalar theory," *J. Opt. Soc. Amer. A, Opt. Image Sci.*, vol. 4, no. 4, pp. 651–654, 1987.
- [9] H. Ringermacher and L. R. Mead, "Comment on observation of superluminal behaviors in wave propagation," *Phys. Rev. Lett.*, vol. 87, no. 5, p. 4830, Jul. 2001.
- [10] G. M. Gehring, A. Schweinsberg, C. Barsi, N. Kostinski, and R. W. Boyd, "Observation of backward pulse propagation through a medium with a negative group velocity," *Science*, vol. 312, no. 5775, pp. 895–897, 2006.
- [11] R. T. Glasser, U. Vogl, and P. D. Lett, "Stimulated generation of superluminal light pulses via four-wave mixing," *Phys. Rev. Lett.*, vol. 108, no. 17, 2012, Art. no. 173902.
- [12] J. K. Ranka, R. S. Windeler, and A. J. Stentz, "Visible continuum generation in air-silica microstructure optical fibers with anomalous dispersion at 800 nm," *Opt. Lett.*, vol. 25, no. 1, pp. 25–27, 2000.
- [13] J. C. Knight, J. Arriaga, T. A. Birks, A. Ortigosa-Blanch, W. J. Wadsworth, and P. S. J. Russell, "Anomalous dispersion in photonic crystal fiber," *IEEE Photon. Technol. Lett.*, vol. 12, no. 7, pp. 807–809, Jul. 2000.
- [14] C. Garrett and D. McCumber, "Propagation of a Gaussian light pulse through an anomalous dispersion medium," *Phys. Rev. A, Gen. Phys.*, vol. 1, no. 2, 1970, Art. no. 305.
- [15] S. Chu and S. Wong, "Linear pulse propagation in an absorbing medium," *Phys. Rev. Lett.*, vol. 48, no. 11, p. 738, 1982.
- [16] H. Shin, "Reducing pulse distortion in fast-light pulse propagation through an erbium-doped fiber amplifier," *Opt. Lett.*, vol. 32, no. 8, pp. 906–908, 2007.
- [17] R. W. Boyd, "Slow and fast light: Fundamentals and applications," *J. Modern Opt.*, vol. 56, nos. 18–19, pp. 1908–1915, 2009.
- [18] G. S. Pati, M. Salit, K. Salit, and M. S. Shahriar, "Demonstration of a tunable-bandwidth white-light interferometer using anomalous dispersion in atomic vapor," *Phys. Rev. Lett.*, vol. 99, no. 13, Sep. 2007, Art. no. 133601.
- [19] M. S. Shahriar, G. S. Pati, R. Tripathi, V. Gopal, M. Messall, and K. Salit, "Ultrahigh enhancement in absolute and relative rotation sensing using fast and slow light," *Phys. Rev. A, Gen. Phys.*, vol. 75, no. 5, May 2007, Art. no. 053807.
- [20] H. Boukellal, Š. Selimović, Y. Jia, G. Cristobal, and S. Fraden, "Simple, robust storage of drops and fluids in a microfluidic device," *Lab Chip*, vol. 9, no. 2, pp. 331–338, 2009.
- [21] R. Jiang, J. Wang, and Y. Guan, "Robust unit commitment with wind power and pumped storage hydro," *IEEE Trans. Power Syst.*, vol. 27, no. 2, pp. 800–810, May 2012.
- [22] M. J. Allen, V. C. Tung, and R. B. Kaner, "Honeycomb carbon: A review of graphene," *Chem. Rev.*, vol. 110, no. 1, pp. 132–145, 2009.
- [23] A. A. Balandin, "Thermal properties of graphene and nanostructured carbon materials," *Nature Mater.*, vol. 10, no. 8, pp. 569–581, Aug. 2011.
- [24] K. S. Novoselov, "Electric field effect in atomically thin carbon films," *Science*, vol. 306, no. 5696, pp. 666–669, Oct. 2004.
- [25] A. K. Geim and K. S. Novoselov, "The rise of graphene," in *Nanoscience and Technology: A Collection of Reviews from Nature Journals*. Singapore: World Scientific, 2010, pp. 11–19.
- [26] L. Ju, "Graphene plasmonics for tunable terahertz metamaterials," *Nature Nanotechnol.*, vol. 6, no. 10, 2011, Art. no. 630.
- [27] B. Wang, X. Zhang, F. J. García-Vidal, X. Yuan, and J. Teng, "Strong coupling of surface plasmon polaritons in monolayer graphene sheet arrays," *Phys. Rev. Lett.*, vol. 109, no. 7, Aug. 2012, Art. no. 073901.
- [28] Z. Fei, A. S. Rodin, G. O. Andreev, W. Bao, A. S. McLeod, M. Wagner, L. M. Zhang, Z. Zhao, M. Thiemens, G. Dominguez, M. M. Fogler, A. H. C. Neto, C. N. Lau, F. Keilmann, and D. N. Basov, "Gate-tuning of graphene plasmons revealed by infrared nano-imaging," *Nature*, vol. 487, no. 7405, pp. 82–85, Jul. 2012.
- [29] G. X. Ni, A. S. McLeod, Z. Sun, L. Wang, L. Xiong, K. W. Post, S. S. Sunko, B.-Y. Jiang, J. Hone, C. R. Dean, M. M. Fogler, and D. N. Basov, "Fundamental limits to graphene plasmonics," *Nature*, vol. 557, no. 7706, pp. 530–533, May 2018.
- [30] A. Woessner, M. B. Lundeberg, Y. Gao, A. Principi, P. Alonso-González, M. Carrega, K. Watanabe, T. Taniguchi, G. Vignale, M. Polini, J. Hone, R. Hillenbrand, and F. H. L. Koppens, "Highly confined low-loss plasmons in graphene–boron nitride heterostructures," *Nature Mater.*, vol. 14, no. 4, pp. 421–425, Apr. 2015.
- [31] J. Chen, M. Badioli, P. Alonso-González, S. Thongrattanasiri, F. Huth, J. Osmond, M. Spasenović, A. Centeno, A. Pesquera, P. Godignon, A. Z. Elorza, N. Camara, F. J. G. de Abajo, R. Hillenbrand, and F. H. L. Koppens, "Optical nano-imaging of gate-tunable graphene plasmons," *Nature*, vol. 487, no. 7405, pp. 77–81, Jul. 2012.
- [32] A. Vakil and N. Engheta, "Transformation optics using graphene," *Science*, vol. 332, no. 6035, pp. 1291–1294, Jun. 2011.
- [33] L. Nucara, F. Greco, and V. Mattoli, "Electrically responsive photonic crystals: A review," *J. Mater. Chem. C*, vol. 3, no. 33, pp. 8449–8467, 2015.
- [34] L. Xiong, "Photonic crystal for graphene plasmons," *Nature Commun.*, vol. 10, no. 1, pp. 1–6, 2019.
- [35] B. Shi, W. Cai, X. Zhang, Y. Xiang, Y. Zhan, J. Geng, M. Ren, and J. Xu, "Tunable band-stop filters for graphene plasmons based on periodically modulated graphene," *Sci. Rep.*, vol. 6, no. 1, p. 26796, Jun. 2016.
- [36] M. Jablan, H. Buljan, and M. Soljačić, "Plasmonics in graphene at infrared frequencies," *Phys. Rev. B, Condens. Matter*, vol. 80, no. 24, Dec. 2009, Art. no. 245435.
- [37] P.-Y. Chen and A. Alà, "Atomically thin surface cloak using graphene monolayers," *ACS Nano*, vol. 5, no. 7, pp. 5855–5863, Jul. 2011.
- [38] H. Lu, C. Zeng, Q. Zhang, X. Liu, M. M. Hossain, P. Reineck, and M. Gu, "Graphene-based active slow surface plasmon polaritons," *Sci. Rep.*, vol. 5, no. 1, Jul. 2015, Art. no. 8443.
- [39] Z. Lu and D. W. J. O. E. Prather, "Calculation of effective permittivity, permeability, and surface impedance of negative-refraction photonic crystals," *Opt. Express*, vol. 15, no. 13, pp. 8340–8345, 2007.



LIQIANG ZHUO is currently pursuing the master's degree with Huaqiao University. He has authored or coauthored over five articles. His research interests include photonic devices and topological plasmonics.



SHAOJIAN SU received the B.S. degree in microelectronics from Shandong University, Jinan, China, in 2007, and the Ph.D. degree in microelectronics and solid state electronics from the Institute of Semiconductors, CAS, Beijing, in 2012. He is currently an Associate Professor with Huaqiao University. He has authored or coauthored over 40 articles in refereed journals. His research interests include semiconductor epitaxy, optoelectronics and microelectronics, and topological photonics.



ZEYANG ZHAO is currently pursuing the master's degree with Huaqiao University. He has authored or coauthored over ten articles. His research interests include photonic devices and topological plasmonics.



HENGJIE ZHOU is currently pursuing the master's degree with Huaqiao University. He has authored or coauthored over ten articles. His research interests include photonic devices and topological plasmonics.



ZHEN HE is currently pursuing the master's degree with Huaqiao University. He has authored or coauthored over five articles. His research interests include photonic devices and topological plasmonics.



HUANXI MA is currently pursuing the master's degree with Huaqiao University. She has authored or coauthored over five articles. Her research interests include photonic devices and topological plasmonics.



ZHILI LIN (Senior Member, IEEE) received the B.S. and Ph.D. degrees in optical engineering from the Department of Optical Engineering, Zhejiang University, Hangzhou, China, in 2002 and 2007, respectively. He is currently a Professor with Huaqiao University. He has authored or coauthored over 100 articles in refereed journals. He holds 12 invention patents. His research interests include computational electromagnetics and computational photonics. He is a Senior Member of the Optical Society of America (OSA) and the International Society for Optics and Photonics (SPIE).



WEIBIN QIU (Senior Member, IEEE) received the Ph.D. degree in microelectronics and solid state electronics from the Institute of Semiconductors, CAS, Beijing, in 2003. He is currently a Professor with Huaqiao University. He has authored or coauthored over 150 articles in refereed journals. He holds two invention patents. His research interests include semiconductor electronic device, photonic devices, circuit and systems, metamolecules, and topological plasmonics. He is a member of the Optical Society of America (OSA).

...